



ARCHIVES  
 of  
 FOUNDRY ENGINEERING

ISSN (2299-2944)  
 Volume 21  
 Issue 3/2021

70 – 80

10.24425/afe.2021.138668

11/3

Published quarterly as the organ of the Foundry Commission of the Polish Academy of Sciences

# Investigation of Particle Filtration in Aluminium Alloy

**B. Baumann<sup>a,\*</sup>, A. Keßler<sup>a</sup>, E. Hoppach<sup>a</sup>, G. Wolf<sup>a</sup>, M. Szucki<sup>a</sup>, O. Hilger<sup>b</sup>**

<sup>a</sup>Foundry Institute, Technische Universität Bergakademie Freiberg,  
 4 Bernhard-von-Cotta-Str., 09599 Freiberg, Germany

<sup>b</sup>Simcast GmbH, Westring 401, 42329 Wuppertal, Germany

\* Corresponding author. E-mail address: Benedict.Baumann@gi.tu-freiberg.de

Received 11.06.2021; accepted in revised form 30.08.2021

## Abstract

The objective of this work is to gain a deeper understanding of the separation effects and particle movement during filtration of non-metallic inclusions in aluminum casting on a macroscopic level. To understand particle movement, complex simulations are performed using Flow 3D. One focus is the influence of the filter position in the casting system with regard to filtration efficiency. For this purpose, a real filter geometry is scanned with computed tomography (CT) and integrated into the simulation as an STL file. This allows the filtration processes of particles to be represented as realistically as possible. The models provide a look inside the casting system and the flow conditions before, in, and after the filter, which cannot be mapped in real casting tests. In the second part of this work, the casting models used in the simulation are replicated and cast in real casting trials. In order to gain further knowledge about filtration and particle movement, non-metallic particles are added to the melt and then separated by a filter. These particles are then detected in the filter by metallographic analysis. The numerical simulations of particle movement in an aluminum melt during filtration, give predictions in reasonable agreement with experimental measurements.

**Keywords:** Simulation, Casting, Filtration, Particle movement, Castings defects

## 1. Introduction

The reactivity of the liquid aluminum leads to the formation of exogenous and endogenous non-metallic inclusions in the melting and casting process. Endogenous inclusions are all non-metallic particles that form in-situ in the melt by chemical reactions, for example, oxides. Exogenous inclusions are particles that are introduced into the melt from outside, e.g. CaO through abrasion of the furnace material [1]. Inclusions impair the mechanical and casting properties of castings and can result in additional work and rejects during machining. In particular, the dynamic strengths are impaired significantly. The inclusion content can be reduced in the melting process by degassing or quiet treatment. In addition, filters in the casting system make it

possible to clean the alloy noticeably during casting, i.e. directly before filling the mold. Ceramic foam filters are used for this. They operate on the principle of depth filtration, i.e. contaminations smaller than the pore diameter reach the filter cross-section and deposit on the filter wall inside the filter. Their structure also causes laminar flow in the gating system and therefore prevents oxide formation and erosion of the mold material. In foundry practice, implementation of the ceramic foam filter in the casting system is generally a question of space on the pattern plate. It does not follow any defined rules, but instead is at best guided by the design recommendations of the filter manufacturers. The filtration process itself is not considered in depth in conventional casting simulations.

The behaviour of particles present in various foundry alloys (both inclusions and intentionally added particles - e.g.

reinforcing phase in Metal Matrix Composite (MMC) composites) and their influence on the properties of the casting are the subjects of many works covering numerical and mathematical modelling [2-6] These studies concern various stages of the production of castings, starting from the melting of materials and ending with the formation of the microstructure. However, the process of in-mold filtration of particles existing in the liquid metal is generally merely considered to be a “black box”, which is defined with a few flow-relevant parameters.

Even in foundry research, until now simulations have mainly been used to verify the influence of the filter on the flow behaviour of the melt and thus on the design of the casting system. The filter in the casting system or the filter action is hardly considered and consequently, there is very little discussion of it in the literature. For example, Foseco [7] describes the correspondence of simulations and his own tests with regard to the filling time and inflow behaviour of melts in the casting mold. Barkhudarov [8] simulates the formation of defects due to turbulent mold filling and uses Flow-3D to track the particles created. Zadeh and Campbell [9] go a step further and compare simulation results from MagmaSoft and Flow-3D with the results obtained from casting tests. The reason they give for the lack of correspondence between the simulation and real tests is that the simulation programs do not take into consideration the oxide skin on the melt and on the melt front. Furthermore, they criticize that the simulation programs ignore the cooling of the metal by the filter with progressing pouring time. This ignores real problems that can lead to filter failure, for example, partial solidification on the melt front when it impinges on the filter or the freezing of the alloy in the filter in case of insufficient overheating of the melt. Simulations by Gebelin [10] deal with optimizing the transverse flow and the filter chamber in order to improve the upstream conditions and to utilize the filter area more optimally. A very different approach is used, for example, by Acosta et al. [11-13] and Werzner, Demuth et al. [14, 15]. They simulate the processes in a few pores or sections of the filter. The computational fluid dynamic (CFD) simulations are focused on the flow of the melt in the pore and the effect of the flow on the deposition of non-metallic contaminations on the pore wall. The consideration is solely limited to the micro-level so that the overall filter system or the filter in the casting system is ignored. In this work, the filtration process, as well as the particle movement through the filter, is investigated on a macroscopic level. In order to understand particle movement, complex simulations are performed using Flow 3D. One focus is the influence of the filter position in the casting system with regard to filtration efficiency. In the second part of this work, the casting models used in the simulation will be replicated and cast in real casting trials to gain further knowledge about filtration and particle movement

## 2. Simulation

The simulation software Flow-3D was used for the simulations, as it allows implementation of the filter as a separate structure in the geometry. The pressure drop, loss of velocity, and thus the flow control is therefore all directly related to the filter structure. The following parameters are defined for the simulation.

### 2.1. Filter

Real filter geometries are used for the simulations. The template for this is provided by industrially produced standard filters with 20 ppi and 30 ppi and dimensions of 50 x 50 x 22 mm each, which is a typical filter size for in-mold filtration during mold casting. The structural data are acquired in the micro-computed tomography and are converted into an STL dataset. The filter structure used in the geometry is defined in Flow-3D by setting further filter-specific parameters. In detail, these are the surface roughness as well as the drag coefficient, which describes the attachment behaviour of the particles on the filter wall. A drag coefficient of 1 is set for the simulations, which corresponds to an adhesion probability of 100%. Therefore, any particle that comes into contact with the filter wall will stick to it and will not flow into the mold cavity. The surface roughness is used to define the material of the filter. The most common filter material for cast aluminum alloys is alumina. The surface roughness of various filter surfaces was determined by Fankhänel et al [16] and is 1.7  $\mu\text{m}$  for filters made of alumina.

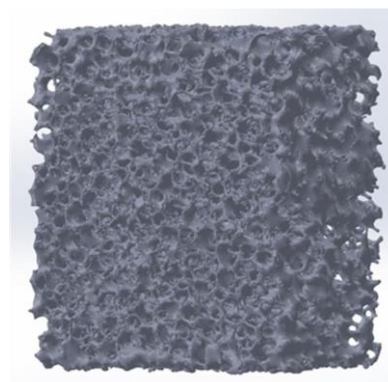


Fig. 1. STL dataset determined in the CT and used in the simulations

### 2.2. Geometry

Figure 2 shows the four different filter geometries and filter positions used in the simulations. The design guidelines of Campbell [17, 18] were used. Moreover, geometries (b) and (d) are adapted to the filter chamber models of Foseco [6].

- the filter is positioned **horizontally** in the runner and the flow approaches it **indirectly**; it is flowed through from the top down (**falling**) (HF)
- the filter is positioned **vertically** in the runner and the flow approaches it **laterally** (V)
- the filter is positioned **horizontally** in the runner and the flow approaches it **indirectly**, it is flowed through from the bottom up (**rising**) (HR)
- the filter is positioned **horizontally** below the sprue and the flow approaches it **directly**; it is flowed through downwards (**falling**) (HFS)

In order to optimize the computing time, only a 10 mm wide strip is simulated instead of the complete filter chamber width.

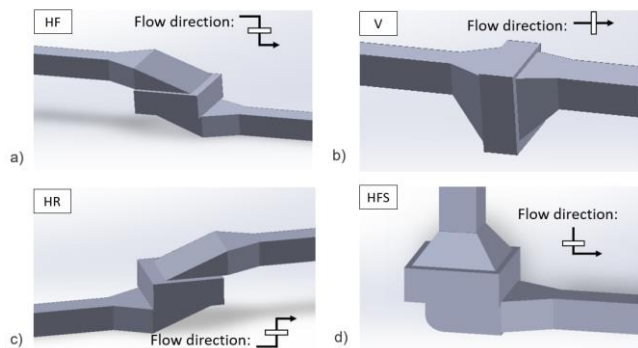


Fig. 2. Examined filter positions a) horizontally falling (HF); b) vertically (V); c) horizontally rising (HR); d) horizontally falling sprue (HFS)

## 2.3. Melt

The aluminum alloy AlSi7Mg0.3 is assumed as the fluid in the simulation. The density is defined with  $2.4 \text{ g/cm}^3$ . The chemical analysis of the melt used in the simulation is shown in Table 5. The pouring temperature and heat transfers between the metal, mold wall, filter, as well as radiation losses to the environment are not considered in the simulation due to computing time savings.

## 2.4. Particles

The number of inclusions to be used for the simulation is set on the basis of the measured values of the LiMCA probe in a test series. An average particle count of 17,500 is determined from more than 140 individual LiMCA measurements. These values were determined in a Collaborative Research Center - CRC 920 project (Multifunctional filters for metal melt filtration) at Constellium [19, 20]. The melt in the test series was deliberately contaminated by adding particles; the values, therefore, do not correspond to the number of inclusions found in melts cast in the foundry industry.

Table 1. Overview of the particles used in the simulations

Type	Density [g/cm <sup>3</sup> ]	Size [μm]	Percentage [%]	Quantity [number]	Particle-ID
Al <sub>2</sub> O <sub>3</sub> (Alumina)	3.95	25	45	7875	1
		35	30	5250	2
		45	7.5	1313	3
		45	7.5	1312	4
MgAl <sub>2</sub> O <sub>4</sub> (Spinel)	3.5	55	5	875	5
		80	5	875	6

Two different particle types are defined in the simulation to look at any difference in the deposition of different particle types. One is alumina as a non-metallic impurity, which is most

common in aluminum alloys. The other is spinel as a non-metallic impurity that occurs very frequently in aluminum alloys due to the manufacturing process. The spinel particles are chosen to be larger than the alumina particles because in reality spinels tend to grow and for this reason are often larger and more massive than the alumina particles. As shown in Figure 3, all defined particles are located in a pile in front of the filter chamber. From this defined position, the particles start to move together with the melt at the beginning of the simulation. Apart from the density, particle size, and number of particles no other parameters can be defined in Flow-3D to describe the particles, such as the shape or surface texture nor do the particles have a temperature. Furthermore, there are no interactions between the particles themselves or between the particles and the mold wall or alloy. Because the particles are much smaller than the pore diameter of the filter and the particles do not interact with each other, only the deep-bed filtration but not the typical filtration mechanisms of sieving and cake filtration [21] can be modelled with the simulation.

## 2.5. Definition of other boundary conditions

To reduce the computing time, the system is described as semi-steady, i.e. in the initial state, only the sprue and the filter chamber are filled with melt. A steady flow state is not reached, as the simulation is stopped after the filtration process is completed. The simulation run time is limited to the duration of the filtration process. The simulation is ended when all the free particles not bound in the filter have left the filter. Figure 3 shows the sequence of a simulation using the filter position HF and a 20 ppi filter. The velocity of the melt is determined by the metallostatic pressure and thus by the geometry of the sprue. It can be considered approximately the same for all filter positions.

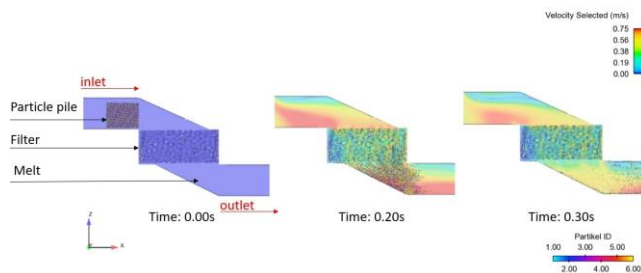


Fig. 3. Example for a sequence of a simulation using the filter position HF and a 20 ppi filter

The filters are additionally divided into nine segments to examine the particles in the filter more closely. The precise number of particles is determined in each filter segment shown in Figure 4 for the filter position HF and V by way of example.

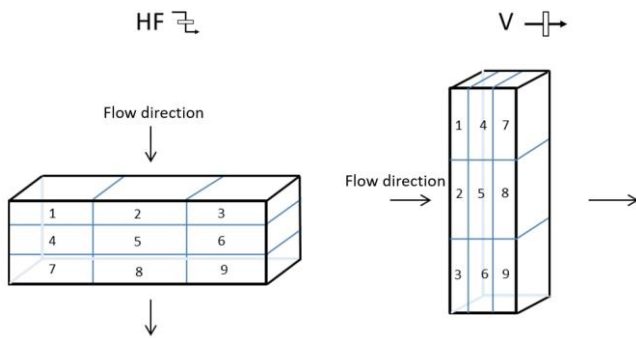


Fig. 4. Filter segmentation

### 3. Results of the simulation

The filtration efficiency  $E$  is calculated from the number of particles upstream and downstream of the filter. This is deemed quality criteria for the filter efficiency and enables direct comparison between the simulations. Where  $N_0$  stands for the number of particles upstream of the filter and  $N_1$  for the number of particles downstream of the filter.

$$E = \frac{N_0 - N_1}{N_0} \times 100 [\%]$$

Table 2 gives an overview of the overall filtration efficiency of all simulations performed. It can be seen that the horizontal filter position in downward flow (HF) has the highest filtration efficiencies, not only with the implementation of a 20 ppi filter but also with a 30 ppi filter. In all filter positions, the increase in particle deposition by using a 30 ppi filter is significant, whereby, in particular, a large increase is registered in a horizontal and directly approached filter.

Table 2.

Filtration efficiencies determined in the simulations

Filter position	20ppi Efficiency	30ppi Efficiency	Percentage increase
HF 	27.9%	36.8%	31.9%
V 	22.7%	33.2%	46.3%
HR 	23.4%	29.5%	26.1%
HFS 	20.8%	33.2%	59.6%

#### 3.1. Influence of particle size on filtration efficiency

For the evaluation of the influence of the filter position on the filtration efficiency of the different particle classes (see Tab. 1), the four filter positions are compared with regard to their filtration efficiency. Figures 5 and 6 clearly show that the filtration efficiency of the 30 ppi filters is significantly higher than that of the 20 ppi filters. Furthermore, in the simulation of the 20 as well as 30 ppi filter, the filter layer HF is always the most effective over the different particle size classes. For the 20 ppi filters, there

is little difference in efficiency between particle sizes from 25  $\mu\text{m}$  to 80  $\mu\text{m}$ . For the 30 ppi filters, the efficiency differs little between particle sizes from 25  $\mu\text{m}$  to 55  $\mu\text{m}$ . Only in the particle size class of 80  $\mu\text{m}$  is an increase in efficiency visible and relevant. The selected increases in particle size are likely too small to be reflected in the filtration efficiency. The ratio of particle size to pore diameter does not change sufficiently to increase the contact of the particles with the filter in the simulation. It is expected that a higher filtration rate will be achieved for particles larger than 80  $\mu\text{m}$ .

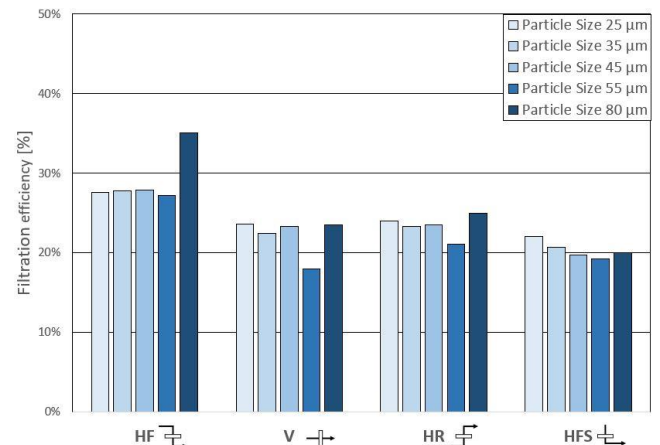


Fig. 5. Filtration efficiency of the different filter positions for the various particle sizes for the simulations with a 20 ppi filter

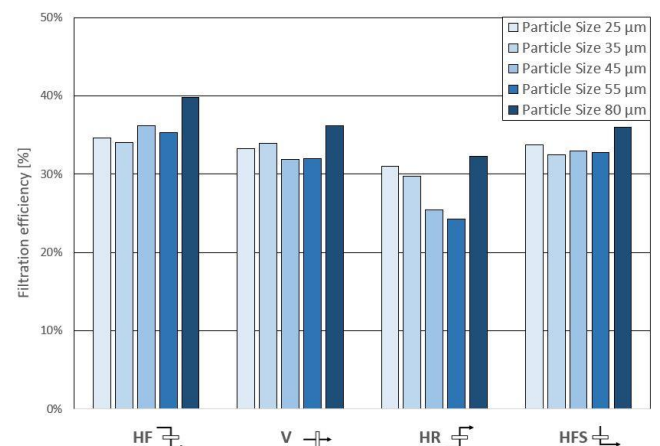


Fig. 6. Filtration efficiency of the different filter positions for the various particle sizes for the simulations with a 30 ppi filter

#### 3.2. Influence of particle type on filtration efficiency

The particle size of 45  $\mu\text{m}$  was used to investigate whether the particle type influences the filtration efficiency of the filter. For this purpose, the same number of spinel particles and aluminum oxide particles with a size of 45  $\mu\text{m}$  were defined in each

simulation. Table 3 summarizes the results for the separation of the 45  $\mu\text{m}$  using the filter position HFS and HF as an example.

Comparing the efficiencies in the individual simulations, no huge differences are seen between the alumina and spinel particles. The largest difference is at the filter position HF (30 ppi) with a difference of 3.4 percentage points. The different

particles are filtered out with a difference of 1 percentage point on average. The influence of the particle type is thus negligible. Presumably, the density difference of the two selected particle types is too small to cause a difference in filtration efficiency.

Table 3.

Influence of particle type on filtration efficiency at a particle size of 45  $\mu\text{m}$ 

Filter position	Filter porosity	Alumina particles 45 $\mu\text{m}$			Spinel particles 45 $\mu\text{m}$		
		Inlet [#]	Filter [#]	E	Inlet [#]	Filter [#]	E
HF $\leftarrow$	20 ppi	1313	366	27.9%	1313	363	27.7%
HF $\leftarrow$	30 ppi	1313	498	37.9%	1313	453	34.5%
HFS $\leftarrow$	20 ppi	1313	260	19.8%	1313	254	19.4%
HFS $\leftarrow$	30 ppi	1313	431	32.8%	1313	433	32.9%

### 3.3. Deposition of the particles in the filter

In the simulation, the filters were divided into 9 cuboids of equal size (see Fig. 4). The number of particles that deposit was determined in

each of the cuboids. Table 4 shows the percentage of filtered particles in the three predefined planes perpendicular to the flow direction of the simulated melt. In the simulations of filter position HF, the percentage difference between the number of particles deposited in the 20 ppi and 30 ppi filters are between 0.1 and 0.4 percentage points. In the vertical flow position, the percentage difference in the number of particles deposited in the filter lies between 0.6 and 1.8 percentage points. In both cases,

the influence of the ppi number on the location of the particle deposition in the filter can be considered to be negligibly small.

Table 4 also shows that there is a relationship between the location of the particle deposition in the filter and the filter position. In filter position HF the particles preferably deposit in the first third of the filter cross-section. Around 44% of all filtered particles are in the first filter plane. The particle fraction then reduces with increasing filter depth to 31% in plane 2 and 24% in plane 3. The distribution of the deposited particles in the filter position HFS is considerably more uniform. Across the 3 planes, the particles are approximately uniformly distributed.

Table 4.

Percentage of deposited particles in each filter plane, as well as the difference ( $\Delta$ ) between 20 ppi and 30 ppi

Filter position	Filter porosity	Filter plane					
		1		2		3	
		Fraction of filtered particles [%]	$\Delta$	Fraction of filtered particles [%]	$\Delta$	Fraction of filtered particles [%]	$\Delta$
HF $\leftarrow$	20 ppi	44.2	0.4	31.4	0.1	24.4	0.3
HF $\leftarrow$	30 ppi	43.8		31.5		24.7	
HFS $\leftarrow$	20 ppi	35.0	0.6	36.0	1.8	29.0	1.3
HFS $\leftarrow$	30 ppi	35.6		34.2		30.2	

Figure 7 shows the percentage distribution of the deposited particles (see Tab. 1) across the entire filter volume, plotted on the velocity profile of the respective filter cross-section. It can be seen that the particle deposition varies, not only over the filter depth (z-direction) but also across the cross-section (x-direction). In filter position HF, most particles are deposited in the middle zone of the filter. The two edge regions to the left and right of it lie significantly below. The flow velocity in the middle and right-hand zone of the filter is comparable and reduces over the filter depth. The flow velocity in the left-hand zone is considerably lower due to the filter chamber design. Due to a backflow of melt in the downstream areas of the filter support, in several cases, it is possible to talk of “dead zones” because the flow velocity is reduced to almost zero. Despite the different flow conditions, the

two edge zones in filter position HF hardly differ concerning deposition effectiveness, especially in the second and third planes. In the slow edge zone, the particles have more time to deposit on the filter wall, e.g. by sedimentation. In the right-hand edge zone with the higher flow velocity, the particles have little time to deposit; instead, in this, there is a higher mass flow rate of particle-bearing melt. Due to the clear upstream and downstream areas, the middle zone with the largest number of deposited particles is the zone in which the largest proportion of the metal, and thus also particles, can pass the filter or be deposited

Unlike filter position HF, in the vertical filter arrangement (V) the particles distribute in the filter significantly more uniformly. In this particles distribute in the filter significantly more uniformly. In this case, the flow approaches the filter surface

uniformly. The velocity with which the melt hits the filter surface is comparatively constant over the whole area. The uniform velocity across the filter cross-section and the uniform utilization of the filter volume causes the particles to deposit uniformly in the whole filter. In the first two planes, only a small difference in deposition rate can be identified. Only in the final third does it reduce slightly. In total, the planes in the z-direction also have only small differences. Even in the supposedly weaker zone of the bottom third of the filter, comparable deposition rates are

achieved as in the upper regions. The reason for this is presumably the small offset in the downstream area, which acts as a brake and holds back many particles due to their inertia. Furthermore, it is also noticeable that with this geometry, several particles deposit on the taper upstream of the filter chamber. Particles also deposit through sedimentation in the downstream area, whereby this deposition is facilitated by the very low flow velocities.

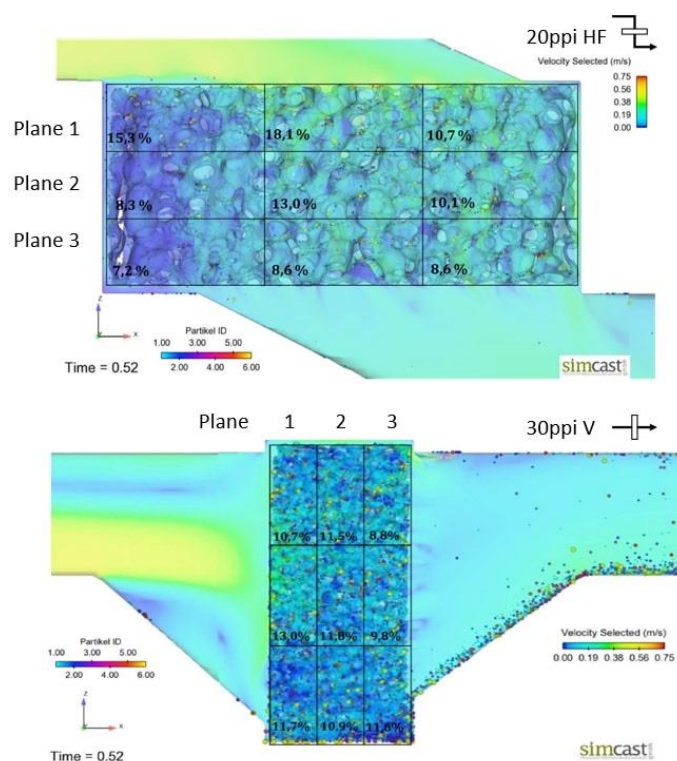


Fig. 7. Distribution of the deposition rate of the particles in percent in the defined areas of the filter, for filter positions HF (20 ppi) and V (30 ppi)

## 4. Casting trial

The results of the simulations show that the filter position and the filter porosity have an influence on the deposition rate of inclusions. It is to be investigated whether this is the case in reality by means of casting trials. For this purpose, foreign particles are intentionally added to a melt and poured into different molds with various filter positions. In order to investigate the behaviour of the particles during filtration, the filters are examined metallographically for their particle content.

### 4.1. Filter

For each casting test, standard alumina foam ceramic filters with dimensions of 50 x 50 x 22 mm and a porosity of 20 and 30

ppi are used. The filters used are from the same manufacturer as the filters that were scanned into CT and used for the simulations.

### 4.2. Geometry

As in the simulations, the filter positions HF, V, HR, and HFS (see Fig. 2) are also examined in the real casting tests. The main objective is to arrange the test setup so that design-related influencing factors are minimized and therefore the results are solely due to the position of the filter in the filter chamber. The design of all casting models is nearly identical and differs only in the design of the filter chamber in the casting system. Figure 8 shows the casting system with a vertical (V) filter position as an example. The molds are made of furan resin bonded molding material.

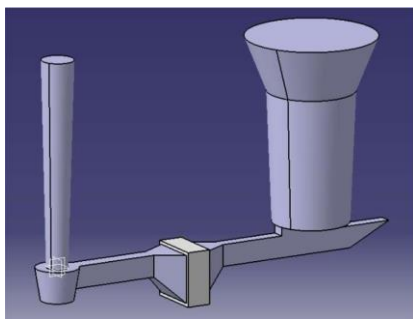


Fig. 8. Filtration efficiency of the different filter positions for the various particle sizes for the simulations with a 30 ppi filter

### 4.3. Melt with foreign particles

As in the simulations, an AlSi7Mg0.3 was used as the base alloy for the casting tests. In order to be able to detect the non-metallic inclusions more easily under the microscope, the melt was refined with strontium. Table 5 shows the chemical analysis of the base alloy. The greatest challenge in the production of the model melt is the insertion of the non-metallic particles into the liquid metal. In order to establish a bond between the melt and the particles, good wetting, i.e. the smallest possible contact angle  $\theta$  between the particles and the aluminum, is necessary. If the contact angle is between  $90^\circ$  and  $180^\circ$ , no wetting takes place. In Damoah et al [22] the contact angle of aluminum melt and  $\text{Al}_2\text{O}_3$  particles is given with  $\theta = 152^\circ$ , the wetting behaviour is therefore insufficient.

There are two ways to create non-metallic impurities in a melt. On the one hand, the particles can be formed in-situ in the liquid aluminum, e.g. by melting recycled material or chips, or on the other hand, the particles can be added to the melt as exogenous inclusions. Exogenous addition of the particles can be done into the furnace or into the casting system. As part of this work, many different methods were tested to create a melt with non-metallic particles. The aim is to obtain a melt with a defined number of non-metallic inclusions of comparable size that can be reproducibly produced. The solution was finally found by the meaning of the use of Duralcan®. Duralcan® is an MMC and is produced by RioTinto Aluminum. Normally MMCs are used for different "high-end" applications like e.g. in the frame of a space shuttle [23]. In the experiments, it is used to selectively introduce foreign particles with a diameter of  $20\ \mu\text{m}$  into the melt. It consists of an aluminum matrix, which is reinforced with  $\text{Al}_2\text{O}_3$  particles. Figure 9 show an overall light microscope image of the used Duralcan® master alloy reinforced with 15 wt-%  $\text{Al}_2\text{O}_3$  particles. There is little to no information from the manufacturer on how the  $\text{Al}_2\text{O}_3$  particles are wetted by the melt. However, own SEM examinations of the particles show that the particles are coated with a thin magnesium layer. The magnesium acts as a kind of adhesion promoter between the particles and the melt. Figure 10 shows an SEM image and phase analysis by EDS mapping at 10000x magnification of the  $\text{Al}_2\text{O}_3$  particles in the Duralcan®. Rajan [24] and Pai [25] also describe the use of magnesium to produce MMCs as a necessary condition.

In further pre-investigations, it was determined that an addition of 3 wt-% Duralcan® is the optimum addition to the melt

so that there are sufficient  $\text{Al}_2\text{O}_3$  particles in the melt for filtration and so that the chemical composition does not differ from the AlSi7Mg base alloy. However, Duralcan® is difficult to introduce homogeneously into the melt and it is not the aim of this work to determine the filtration efficiency of the real casting trials.

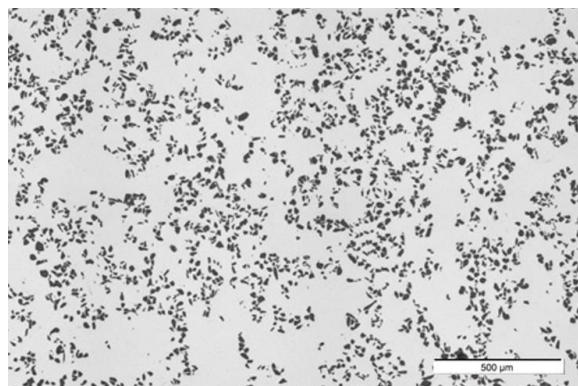


Fig. 9. Overall light microscope image of the structure of the used Duralcan master alloy with 15 wt-%  $\text{Al}_2\text{O}_3$

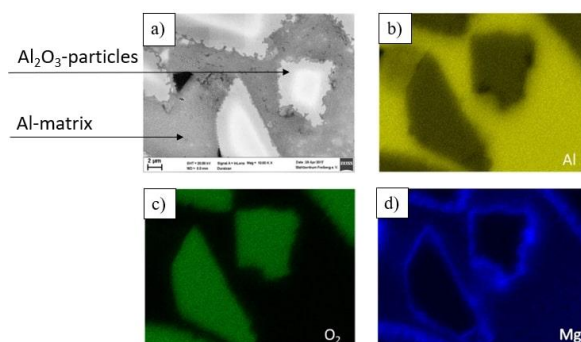


Fig. 10. Results of SEM (a) investigation including EDS analysis of the  $\text{Al}_2\text{O}_3$  particles with EDS signal for the elements aluminum (b), oxygen (c), and magnesium (d)

### 4.4. Execution of the casting trials

The melt is prepared in a 20 kW resistance-heated crucible furnace with a capacity of 30 kg of molten aluminum. For each batch, 27 kg of ingot material of the alloy AlSi7Mg0.3 are melted and subsequently refined with 0.02% strontium and degassed for 20 minutes using an impeller. At  $750^\circ\text{C}$  melting temperature, the 3 wt-% Duralcan®, which corresponds to 0.8 kg Duralcan® on the total melting quantity, is added. Before the metal is transferred from the crucible to the ladle, it is homogenized manually by stirring with a graphite rod. This is intended to distribute the alumina particles evenly in the melt and prevent their sedimentation. When the alloy reaches a temperature of  $730^\circ\text{C}$ , casting takes place. From one crucible filling 8 molds with the same filter chamber, geometry are cast. A spectral sample is taken for each batch to check the chemical composition of the melt. Table 5 shows the average value of all chemical analyses of the

melt. After solidification and cooling of the metal, the casting is removed from the mold and the filter chamber with the filter cast in it is processed for metallographic examinations.

Table 5.

Average chemical compositions in wt% of the melt used for simulation and the melt used for the casting trials before and after adding Duralcan®

	Si	Mg	Fe	Mn	Zn	Sr	Al
	[%]	[%]	[%]	[%]	[%]	[%]	[%]
AlSi7Mg (simulation)	7.00	0.35	0.19	0.100	0.018	-	92.29
AlSi7Mg (without Duralcan®)	7.14	0.27	0.10	0.010	0.010	0.02	92.35
AlSi7Mg (with Duralcan®)	7.02	0.31	0.11	0.003	0.010	0.02	92.31

#### 4.5. Metallographic examinations of the filter

Like the simulations, the filters are also divided into segments, whereby plane 1 and plane 5 are located upstream and downstream of the filter respectively. Individual images of each zone are assembled using a 3D microscope with 200x magnification to form a panorama image and are evaluated by

image analysis. The size, morphology, and appearance of the particles are known from pre-investigations and therefore enable simple identification of the impurities (see Fig 11).

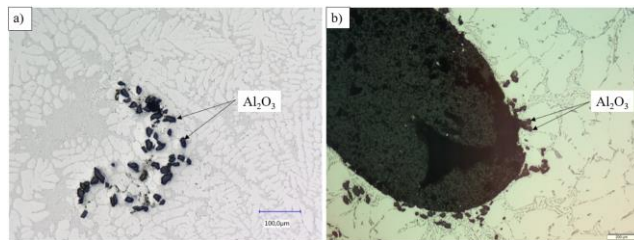


Fig. 11. Comparison of the morphology of the  $\text{Al}_2\text{O}_3$  particles in the melt (left) and in the filter (right), images taken with a light microscope at (a) 100x and (b) 200x magnification respectively

### 5. Results of the casting tests

Figures 12 and 13 show the assembled light microscopy images of filter positions V and HF by way of example. All  $\text{Al}_2\text{O}_3$  particles detected under the microscope are marked red so that the deposition of the particles in the filter can be traced.

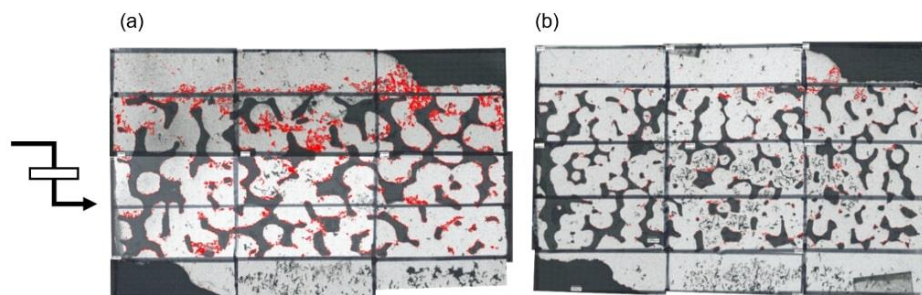


Fig. 12. Examples of the filter evaluation for the HF position for (a) a 20 ppi and (b) a 30 ppi filter

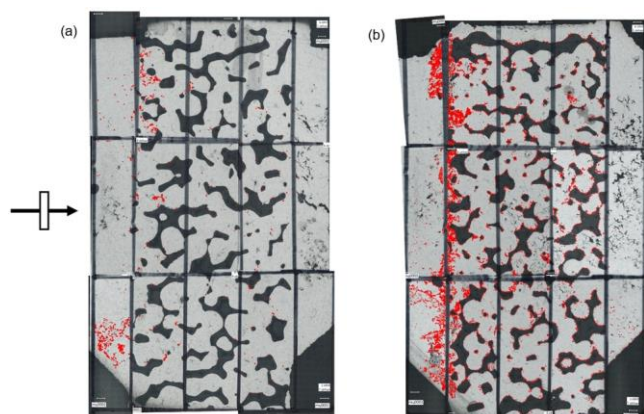


Fig. 13. Examples of filter evaluation of the vertically positioned filter (V) for (a) a 20 ppi and (b) a 30 ppi-filter

Figure 14 shows the average number of particles determined in the defined zones. The colour scale simplifies the identification of particularly active zones in the filter. It can be seen that the number of particles in the horizontal filter position reduces with filter depth. The particles detected in the vertical filter position are significantly more uniformly distributed. The metallographic evaluation of the filters can be used to define regions that facilitate particle deposition. These zones are represented in greater detail in the following:

As shown by way of example in Figure 15, the  $\text{Al}_2\text{O}_3$  particles deposit almost solely near the filter bridge and form a rim around the filter bridge. However, the particles very rarely adhere directly to the filter wall but instead are often located several micrometers away from it. Consequently, in the aluminum melt, there is no direct reaction between the particles and the filter wall, which attaches the particles to the filter and therefore removes them from the melt. However, as considerably fewer particles were

counted inside the pores themselves than near the filter bridge, it seems evident that surface forces are working.

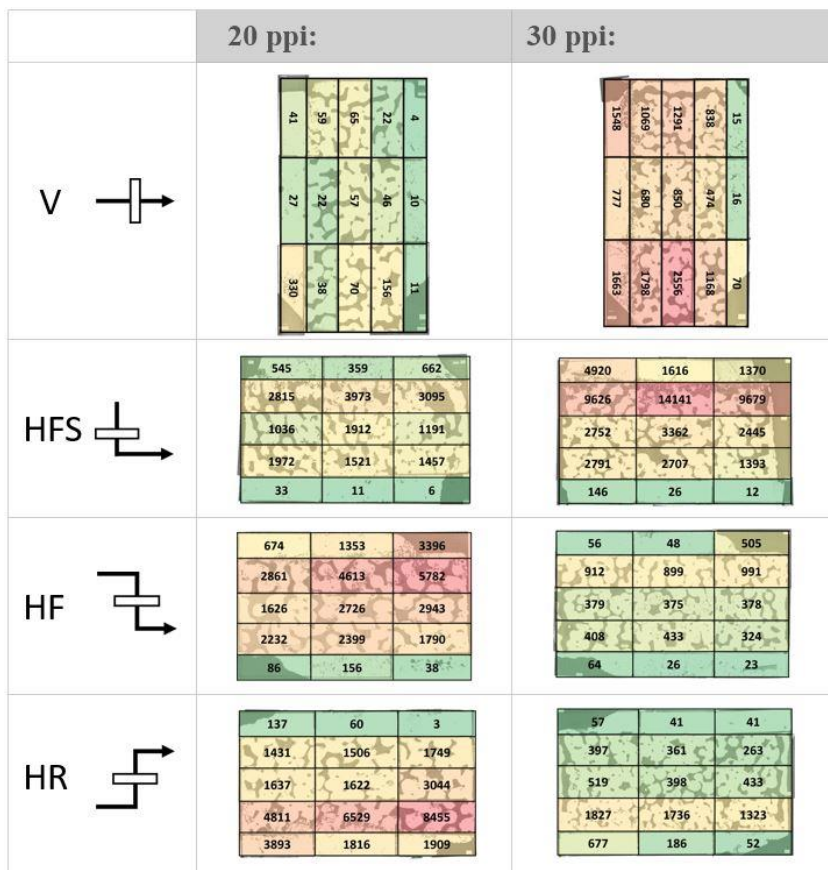


Fig. 14. Average number of particles in the individual areas of the filter

The  $Al_2O_3$  particles preferably deposit in the inflow area of the filter, i.e. in the first third of the filter. The deposition is comparable with the mechanism of precoat filtration. As the  $Al_2O_3$  particles all lie within a uniform size range and are considerably smaller than the pore diameter, they alone cannot block the pores of the filter. The evaluation of the filter showed that, in the upper zone of the filter, endogenous inclusions, such as alumina skins or spinels often function as a type of collector (see Fig 16 and Fig 17). On the one hand, these considerably larger impurities block the filter pores and therefore hold back the added  $Al_2O_3$  particles, on the other hand, the  $Al_2O_3$  particles preferably adhere to these non-metallic impurities and lead to large agglomerates. This phenomenon occurs especially with the filter position V and HFS. One reason for this could be stronger turbulence of the melt when it directly hits the filter and thus leads to the generation of endogenous particles.

The filter is held in the correct position in the sand mold by filter prints. In the evaluation, it is noticeable that the  $Al_2O_3$  particles deposit preferably in the zones below and above the filter prints. I.e. the majority of the particles do not deposit in the middle filter zone but the edge zone of the filter. The numbers in Figure 14 show that this observation applies to all tests, except the HFS position. The reason is probably the backing-up effect of the melt on the prints. Once the metal has penetrated this zone of the

filter, the filter prints prevent unobstructed flowing off of the melt. The inertia of the particles and the comparatively long dwell time of the melt in these zones facilitate deposition of the non-metallic impurities. When the filters are positioned horizontally, directly under the sprue (HFS), the melt hits the filter with very high velocity. As a result, the middle filter zone is presumably impacted considerably more than the edge zones, so that a larger number of particles was also counted here.

### 5.1. Particle movement assessment

Both in the simulation and the real casting tests, the movement of the non-metallic particles through the filter was examined. In the simulation, the particle movement can be followed directly. In the casting trials, conclusions can be drawn about the particle movement based on the examined filters. The aim of this work was never to compare the simulation using Flow 3D with reality. The fact that the particles in the simulation do not influence each other alone shows that there is still a lot of development work to be done by the software programmers before a real casting test can be simulated to evaluate separation efficiencies by means of filtration.

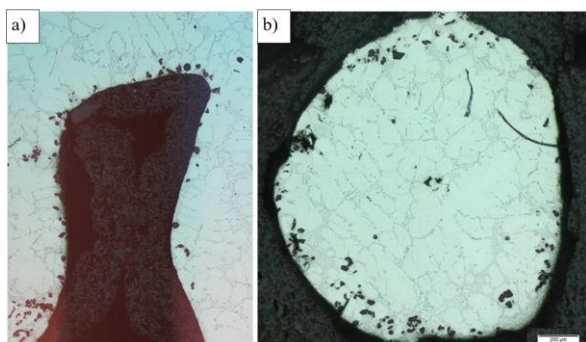


Fig. 15. (a) Deposition of the  $\text{Al}_2\text{O}_3$  particles on a filter bridge; (b) Look inside a pore with the deposition of the  $\text{Al}_2\text{O}_3$  particles near the filter wall and an impurity-free pore centre; Image taken using the light microscope with 50x magnification

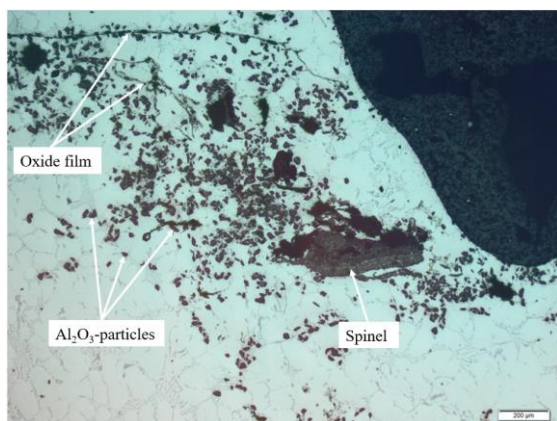


Fig. 16. Upstream area of a filter in position HFS in which endogenous inclusions serve as collectors for  $\text{Al}_2\text{O}_3$  particles; light microscope with 50x magnification

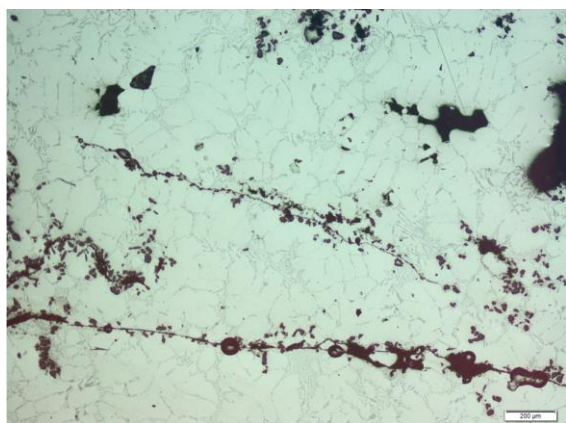


Fig. 17.  $\text{Al}_2\text{O}_3$  particles strung together like pearls on oxide skins, light microscope with 50x magnification

It should be mentioned that good correspondence between the simulation results and real casting trials exists. The results of both the simulation and the real casting tests indicate that the particles

are deposited more in the first third of the filter, regardless of the filter porosity or the filter position in the casting system.

Real phenomena during the casting tests lead to the fact that the results of the simulation and the casting tests do not coincide in some areas of the filter. For example, it is not possible to take the build-up and entry of oxide skins before the filter into account in the simulation, resulting in particles attaching to the oxide skins upstream of the filter.

## 6. Conclusion

Numerical simulations of particle motion in an aluminum melt during filtration, give predictions in reasonable agreement with experimental measurements. In both the simulation and the casting tests, the particles show a similar flow behaviour through the filter. The differences between the simulations and the measured data are due to many phenomena during the casting tests e.g. that the particles have different shapes and surface textures, which cannot yet be captured in simulations. As technology improves, it will be possible in the future to create better and more accurate simulations for melt filtration that take e.g. the interaction of the particles with each other into account. The following conclusions are drawn from the study:

- The simulation as well as the casting tests have shown that the  $\text{Al}_2\text{O}_3$  particles stick to the  $\text{Al}_2\text{O}_3$  filter walls.
- The  $\text{Al}_2\text{O}_3$  particles stick to  $\text{Al}_2\text{O}_3$  surfaces. Regardless of whether it is a ceramic foam filter made of  $\text{Al}_2\text{O}_3$  or a free surface in the form of an oxide skin.
- For further filtration simulations with Flow 3D, the drag coefficient can be set to 1.
- The simulation shows a higher separation rate of particles when using a 30 ppi filter compared to a 20 ppi filter. This observation was also found in reality.
- For the production of MMCs with  $\text{Al}_2\text{O}_3$  particles, coating of the particles with magnesium is indispensable

## Acknowledgments

Funded by the Deutsche Forschungsgemeinschaft (DFG, German Research Foundation) – Project-ID 169148856 – SFB 920.

## References

- [1] Hasse, S. (2008). *Foundry lexicon*. Berlin: Fachverlag Schiele & Schön GmbH. (in German).
- [2] Waz, E., Bansal, A., Chapelle, P., Delannoy, Y., Bellot, J.P. & Le Brun P. (2016). Modeling of inclusion behavior in an aluminum induction furnace. In Williams E. (Eds.) *Light Metals 2016* (pp. 849-854). Springer, Cham. [https://doi.org/10.1007/978-3-319-48251-4\\_144](https://doi.org/10.1007/978-3-319-48251-4_144).
- [3] Kroll-Rabotin, J.-S., Gisselbrecht, M., Ott, B., May, R., Fröhlich, J. & Bellot, J.-P. (2020). Multiscale simulation of non-metallic inclusion aggregation in a fully resolved bubble

- swarm in liquid steel. *Metals*, 10(4), 517. <https://doi.org/10.3390/met10040517>.
- [4] Żak, P.L., Kalisz, D., Lelito, J., Szucki, M., Gracz, B. & Suchy, J.S. (2015). Modelling of non-metallic particles motion process in foundry alloys. *Metallurgija*. 54(2), 357-360.
- [5] Szucki, M., Kalisz, D., Lelito, J., Żak, P.L., Suchy, J.S. & Krajewski, W. K. (2015). Modelling of the crystallization front – particles interactions in ZnAl/(SiC)p composites. *Metallurgija*. 54(2), 375-378.
- [6] Lelito, J., Żak, P.L., Greer, A.L., Suchy, J.S., Krajewski, W.K., Gracz, B., Szucki, M. & Shirzadi, A.A. (2012). Crystallization model of magnesium primary phase in the AZ91/SiC composite. *Composites. Part B, Engineering*. 43(8), 3306-3309.
- [7] Jäckel, E. (2019). *Influence of filter structure and casting system on the filtration efficiency in Aluminum Mold Casting*. Unpublished doctoral dissertation, Technische Universität Bergakademie Freiberg. (in German)
- [8] Barkhudarov, M.R., Hirt, C. W. (1998). Tracking defects. Flow Science, Inc. Retrieved May 26, 2021, from <https://www.flow3d.com/wp-content/uploads/2014/08/Tracking-Defects.pdf>.
- [9] Zadeh, A. & Campbell, J. (2003). Metal flow through a filter system. *AFS Transaction*. 02-020, 1-17.
- [10] Gebelin, J. & Jolly, M. (2002). Modelling filters in light alloy casting processes (or "What really happens when aluminium flows through a filter"). *AFS Transaction*. 110, 109-119.
- [11] Acosta, G.F.A. & Castillejos, E.A.H. (2000). A mathematical model of aluminum depth filtration with ceramic foam filters: Part I. Validation for short-term filtration. *Metallurgical and Materials Transactions B*. 31, 491-502. DOI: 10.1007/s11663-000-0155-3.
- [12] Acosta, G.F.A. & Castillejos, E.A.H. (2000). A mathematical model of aluminum depth filtration with ceramic foam filters: Part II. Application to long-term filtration. *Metallurgical and Materials Transactions B*. 31, 503-514. DOI: 10.1007/s11663-000-0156-2.
- [13] Acosta, G.F.A., Castillejos, E.A.H., Almanza, R.J.M. & Flores, V.A. (1995). Analysis of liquid flow through ceramic porous media used for molten metal filtration. *Metallurgical and Materials Transactions B*. 26, 159-171. DOI: 10.1007/BF02648988.
- [14] Werzner, E., Abendroth, M., Demuth, C., Settgast, C., Trimis, D., Krause, H. & Ray, S. (2017). Influence of foam morphology on effective properties related to metal melt filtration. *Advanced Engineering Materials*. 19(9), 1700240. DOI: 10.1002/adem.201700240.
- [15] Demuth, C., Werzner, E., Mendes, M., Krause, H., Trimis, D. & Ray, S. (2017). Non-Isothermal simulations of aluminium depth filtration. *Advanced Engineering Materials*. 19(9), 1700238. DOI: 10.1002/adem.201700238.
- [16] Fankhänel, B., Stelter, M., Voigt, C. & Aneziris, C. G. (2017). Interaction of AlSi7Mg with oxide ceramics. *Advanced Engineering Materials*. 19(9), 1700084. DOI: 10.1002/adem.201700084.
- [17] Campbell, J. (1991). *Castings*. Oxford: Butterworth-Heinemann Ltd.
- [18] Campbell, J. (2011). *Complete casting handbook: metal casting processes, metallurgy, techniques and design*. Oxford: Butterworth-Heinemann Ltd.
- [19] Voigt, C., Jäckel, E., Taina, F., Zienert, T., Salomon, A., Wolf, G., Aneziris, C. G. & Le Brun, P. (2017). Filtration efficiency of functionalized ceramic foam filters for aluminium melt filtration. *Metallurgical and Materials Transactions B*. 48(1), 497-505. DOI: 10.1007/s11663-016-0869-5.
- [20] Le Brun, P., Taina, F., Voigt, C., Jäckel, E., Aneziris, C. G. (2016). Assessment of active filters for high quality aluminium cast products. In E. Williams (Eds.), *Light Metals 2016* (pp. 785-789). Basel: Springer International Publishing.
- [21] Olson III, R.A. & Martins, L.C.B. (2005). Cellular ceramics in metal filtration. *Advanced Engineering Materials*. 7(4), 187-192. DOI: 10.1002/adem.200500021.
- [22] Damoah, L.N.W. & Zhang, L. (2010). removal of inclusions from aluminum through filtration. *Metallurgical and Materials Transactions B*. 41(4), 886-907. DOI: 10.1007/s11663-010-9367-3.
- [23] Beffort, O. (2002). Metal matrix composites: properties, applications and machining (in German), in 6. Internationales IWF-Kolloquium, 18-19 April 2002 (pp. 43-52). Egerkingen, Schweiz: ETH Zürich.
- [24] Pai, B.C., Pillai, R. & Satyanarayana, K. (1993). Stir cast aluminium alloy matrix composites. *Key Engineering Materials*. 79-80, 117-128. DOI: 10.4028/www.scientific.net/KEM.79-80.117.
- [25] Rajan, T.P.D., Pillai, R.M. & Pai, B.C. (1998). Reinforcement coatings and interfaces in aluminium metal matrix composites. *Journal of Material Science*. 33, 3491-3503. DOI: 10.1023/A:1004674822751.